Available online at www.sciencedirect.com
ScienceDirect
Applied Catalysis A: General 338 (2008) 58–65
APPLIED CATALYSIS A: GENERAL
www.elsevier.com/locate/apcata

Supercritical deposition of Pt on SnO_2-coated Al_2O_3 foams: Phase behaviour and catalytic performance

G. Incera Garrido [a], F.C. Patcas [a,*], G. Upper [b], M. Türk [b], S. Yilmaz [c], B. Kraushaar-Czarnetzki [a]

[a] Institute of Chemical Process Engineering CVT, University of Karlsruhe, Kaiserstrasse 12, D-76128 Karlsruhe, Germany
[b] Institute of Technical Thermodynamics and Refrigeration ITTK, University of Karlsruhe, Kaiserstrasse 12, D-76128 Karlsruhe, Germany
[c] Department of Chemical Engineering, Izmir Institute of Technology, Urla 35497, Izmir, Turkey

Received 15 November 2007; received in revised form 14 December 2007; accepted 17 December 2007
Available online 27 December 2007

Abstract

Deposition and reduction of an organometallic platinum complex from a supercritical $Pt(COD)Me_2/CO_2$ solution was carried out to produce Pt/SnO_2 catalysts supported on Al_2O_3 foams for CO oxidation at moderate temperatures. The phase behaviour of the complex in supercritical carbon dioxide was investigated to find the optimum pressure and temperature conditions for the deposition. For the $Pt(COD)Me_2/CO_2$ mixture, the melting point decreased with increasing pressure from 378 K at 0.1 MPa to 360 K at 25.6 MPa. Additional investigations showed that the solubility of $Pt(COD)Me_2$ in CO_2 increases from 5.9×10^{-4} mol/mol at 11.2 MPa and 313 K to 3.4×10^{-3} mol/mol at 29.6 MPa and 353 K. The supercritical deposition yielded catalysts with highly dispersed platinum nanoparticles of approx. 3 nm having a narrow size distribution and thus, a superior activity towards oxidation of carbon monoxide in comparison to a catalyst prepared by the conventional aqueous impregnation of Pt.

Keywords: Supercritical fluid; Platinum; Nanoparticle; CO oxidation; Ceramic foam

1. Introduction

The catalytic oxidation of carbon monoxide is an important purification step downstream to, e.g. reforming and combustion processes. In the context of fuel cell technology, in particular, CO removal gained increasing importance since the catalysts of the low-temperature fuel cells are extremely sensitive to poisoning by CO. Here, the CO concentration needs to be reduced from about 1% to below 10 ppm in the presence of excess hydrogen. The preferential oxidation (PROX) of CO, i.e. the selective oxidation of CO to CO_2 with minimum H_2 consumption, could be an option to reach this goal. However, PROX has to be carried out at low temperatures in order to avoid the occurrence of the reverse water gas shift-reaction which produces CO [1] and, therefore, requires highly active catalysts.

The system Pt/SnO_2 has been studied for many years because it has shown to catalyze the CO oxidation at moderate temperatures, where neither platinum nor tin dioxide alone are catalytically active. The high activity is ascribed to a synergistic bifunctional mechanism in which Pt provides the adsorption sites for CO, while oxygen adsorbs dissociatively on SnO_2 [2,3]. The reaction between the adsorbed species occurs at the Pt/SnO_2 boundary. If this synergistic mechanism holds, it should be of extreme importance for a high catalytic activity to realize a large boundary surface area, i.e. to achieve a high dispersion of the platinum particles on the tin dioxide phase.

The preparation of fine dispersed platinum particles of 1–2 nm size on γ-alumina supports is a well-studied process. The precursor here is chloroplatinic acid and the fine dispersion of platinum is achieved by an intercourse of ion exchange and chloride interaction with the amphoteric carrier. In the case of SnO_2, platinum is usually deposited by means of wet impregnation of the SnO_2 washcoat with aqueous solutions of platinum tetramine nitrate [4]. Owing to the relatively low surface area of SnO_2 and the capillarity effects during drying, the achievement of high Pt dispersions is difficult. Here, we report on the deposition and reduction of an organometallic

* Corresponding author. Tel.: +49 721 608 4134; fax: +49 721 608 6118.
E-mail address: Florina.Patcas@ciw.uni-karlsruhe.de (F.C. Patcas).

0926-860X/$ – see front matter
doi:10.1016/j.apcata.2007.12.019

Table 1
Thermo-physical properties of gases, supercritical fluids, and liquids [6]

	Gas 0.1 MPa, 285–300 K	Supercritical fluid	Liquid 285–300 K
ρ (kg/m^3)	60–200	200–500	600–1600
D_{ij} (cm^2/s)	0.1–0.4	0.7×10^{-3}	$(0.2–2) \times 10^{-5}$
η (Pa s)	$(1–3) \times 10^{-5}$	$(1–3) \times 10^{-5}$	$(0.2–3) \times 10^{-3}$

platinum complex from supercritical solution. This process is known as supercritical fluid reactive deposition (SFRD) [5].

Thermophysical properties of supercritical fluids are between those of gases and liquids: they offer low viscosity (η), high diffusion rate (D_{ij}) and the absence of surface tension (Table 1).

One of the most promising supercritical fluids for many engineering purposes is carbon dioxide. It exhibits low critical pressure and temperature values (T_c = 304.13 K; P_c = 7.38 MPa), low toxicity and is chemically inert. These properties have led to the use of $scCO_2$ in various extractive processes such as the decaffeination of coffee, and to the development of novel methods like SFRD for the preparation of nanostructured materials [7–9]. SFRD not only enables the deposition of Pt nanoparticles in narrow size distributions, it also allows for a homogeneous distribution of the metal on carriers with complex geometric structures or tortuous pore networks where impregnation with liquids tends to yield maldistributions under the effects of gravity, surface tension and capillary forces. In this work, supercritical deposition was applied to produce Pt/SnO_2 catalysts supported on Al_2O_3 foams. In the first section, the thermodynamic behaviour of supercritical Pt-solutions is described. In the second part, we compare $Pt/SnO_2/Al_2O_3$-foam catalysts produced by means of wet-chemical and by supercritical Pt deposition with respect to their physico-chemical properties and to their catalytic activity in the CO oxidation.

2. Experimental

The platinum complex selected for SFRD was dimethyl-(1,5-cyclooctadien)-platinum ($Pt(COD)Me_2$), purchased from Strem Chemicals.

2.1. Phase behaviour of $Pt(COD)Me_2/CO_2$ mixtures

The knowledge of solid–liquid–gas (S–L–G) and solid–fluid (S–F) phase behaviour is important to the understanding and design of processes with supercritical fluids. In the case of the SFRD process, an insufficient solubility of the organometallic precursor limits the practical applicability. In addition, the properties of the produced particles such as particle size, size distribution, and morphology are often strongly influenced by the melting behaviour of the mixtures involved.

2.1.1. Melting point depression

For the determination of the pressure–temperature (p–T) projection of the S–L–G curve, the widely used method has been the first melting point method. This measurement technique was applied because of its simplicity and quickness of operation. Usually, the melting point of Pt(COD) under CO_2 pressure was determined by finding the melting temperature at a constant system pressure. The static equilibrium cell with an inner volume of 3.3 cm^3 is designed for pressures up to 100 MPa and temperatures up to 473 K and is equipped with three sapphire windows (8 mm in diameter), which allow the observation of the solute and the fluid at high pressure. In a typical experiment, the temperature was increased slowly until the onset of melting was observed. Thereby a heating rate of either 0.05 K/min or 0.1 K/min was used and the constant system pressure is adjusted with the manual piston pump.

2.1.2. Solubility

The solubility of $Pt(COD)Me_2$ in CO_2 was determined with a high-pressure variable volume cell. The heatable cell has an internal variable volume that allows changes in cell volume (V = 3.3–7.3 cm^3) and pressure via a movable piston. Two sapphire windows (8 mm in diameter) enable a visual observation of the phase behaviour. Phase separation was defined as the point when precipitation of the solid was observed. Cloud points were determined visually by noting the pressure where the organometallic precipitated out of the solution. Repeated measurements were performed to minimize the influence of kinetic effects on the onset of precipitation. Therefore, the system pressure was slowly reduced in the range from 0.6 MPa/min to 1.2 MPa/min. Each cloud point determination was conducted three times giving reproducibility within ±0.2 MPa.

A more detailed description of both apparatus and the experimental procedure is given in literature [10,11].

2.2. Catalyst preparation

45 PPI α-Al_2O_3 foams (Vesuvius Inc.) were used as supports for the Pt/SnO_2 catalysts. The blank foams were coated with tin dioxide by dipping in a 250 g/L SnO_2 sol. The sol was prepared by dissolving metallic tin in nitric acid, washing repeatedly the resulted precipitate with aqueous ammonia solution and subsequently with distilled water. The precipitate was then dispersed with cyclohexylamine to form a sol. A detailed description can be found elsewhere [12]. The carrier pieces were coated two times in order to ensure full coverage of the surface. Each impregnation was followed by drying at 353 K and calcining at 623 K.

2.2.1. Supercritical fluid reactive deposition of platinum

The setup used for supercritical deposition comprised a deposition vessel connected by pipes and needle valves on both sides to two screw presses for controlled filling of carbon dioxide and hydrogen under pressure. The stainless steel deposition vessel (49 cm^3) was equipped with carbon/PTFE O-rings, thermocouple, pressure transducer, rupture disk, and a ventilation line with filters to prevent loss of solid organic metal complex. Prior to each experiment, $Pt(COD)Me_2$ and 3–5 SnO_2-coated foam pieces were placed into the vessel in two

separate open recipients. A magnetic agitator was placed between the recipients for an enhanced mixing of the sc-solution. In all experiments, the ratio between Pt(COD)Me_2 and the support was kept constant at 0.024 g/g. After assembling the vessel and vacuum degassing, 5 MPa CO_2 was fed into the system. The deposition temperature was then set to avoid condensing of CO_2. Subsequently, the CO_2 pressure was slowly increased until the desired sc-conditions for deposition were reached. Then, the platinum complex started to dissolve in the carbon dioxide and to adsorb on the tin dioxide wash coat. The duration of dissolution and adsorption was 20 h. After adsorption of the complex, 1.17 vol.% hydrogen was added to the mixture at constant temperature and pressure and kept for 2 h. During this process, the complex is reduced and the organic ligands are transformed to cyclooctane and methane. The system was then depressurized slowly to atmospheric conditions and cooled down to ambient temperature. The Pt/SnO_2-loaded foam catalysts were removed and the average mass percentages of deposited platinum were measured gravimetrically (Mettler-Toledo) with an accuracy of ±0.2 mg. The precise platinum contents of the pieces used for catalytic activity tests were determined by means of X-ray fluorescence analysis (Spectrace 5000, 50 kV, Rh Target).

2.2.2. Impregnation with an aqueous platinum solution

In order to compare SFRD catalysts with samples prepared according to a conventional method for platinum loading, SnO_2-coated foams were impregnated with an aqueous solution containing 15 g/L $Pt(NH_4)_4NO_3$ [4,12]. The mass ratio of Pt in the solution to SnO_2 on the support amounted to 2. The coated foams were submerged in the solution, agitated gently and left for 3 h. Then they were removed from the solution, dried at 353 K and calcined at 623 K following the same procedure as after the SnO_2 loading. Prior to use, the Pt was reduced in a flow of 5% H_2/N_2 at 353 K for 2 h. The Pt content of the catalysts was measured via X-ray fluorescence analysis.

2.3. Catalyst characterization

The microstructures of the catalysts from SFRD and aqueous Pt-deposition were investigated by means of scanning electron microscopy (SEM), transmission electron microscopy (TEM), and energy-dispersive X-ray (EDX) analysis. The layer thickness of SnO_2, the surface morphology and element location were investigated with SEM/EDX (LEO 1530). Prior to the examination of the layer thickness, the foam sample was embedded in resin to avoid chipping of the SnO_2 layer and grinded. The platinum distribution on SnO_2 (microstructure) was analyzed using a Philips-CM200-FEG TEM. The microscope was equipped with in situ EDX spectrometer for elemental analysis. Samples for TEM were prepared by milling the catalyst, dispersing in acetone and transferring into a holey carbon film on a copper mesh. The platinum particle size distribution was determined from over 100 images on different locations.

The CO oxidation rates were measured in a tubular, electrically heated glass reactor with external recycle through a membrane pump. To ensure a good mixing (gradientless system), the recycle ratio was kept at 25–30. The reaction rate related to the catalyst bed volume and the first order rate coefficients of the chemical reaction were calculated by mass balancing the system in the steady state as follows:

$$r_V\ (\mathrm{mol}/(\mathrm{m}^3\ \mathrm{s})) = \frac{C_{CO,0}\dot{V}_0}{V_{cat}} X_{CO} \quad (1)$$

$$k_{Pt}(\mathrm{m}^3/(\mathrm{g_{Pt}s})) = \frac{\dot{V}_0}{m_{Pt}} \frac{X_{CO}}{1 - X_{CO}} \quad (2)$$

where $C_{CO,0}$ is the inlet CO concentration, $\dot{V}_0$ is the inlet volume flow rate, V_{cat} is the catalyst bed volume, m_{Pt} is the platinum mass in the catalyst and X_{CO} is the CO conversion. The inlet gas concentration amounted to 1050 vol. ppm CO in air. The gas hourly space velocity of the CSTR-system was kept constant at 300,000 h^{-1}. The concentrations of CO and CO_2 at both, entrance and outlet of the recycle loop were measured with a non-dispersive infrared analyzer (Rosemount Analytical). At constant hydrodynamic conditions and CO inlet concentrations, the temperature was increased from 353 K until external mass transfer limitation was reached.

3. Results and discussion

3.1. Phase behaviour of Pt(COD)Me_2/CO_2 mixtures

3.1.1. Melting point depression

In Fig. 1 the experimental pressure–temperature data for the SLG-line for the binary system Pt(COD)Me_2/CO_2 are depicted. This binary system shows the typical behaviour of a highly asymmetric mixture, consisting of compounds with great differences in size, molecular structure, and intermolecular interactions [13]. Due to the high solubility of CO_2 in the liquid Pt(COD)Me_2, the dp/dT slope of the SLG-line is negative in the pressure range investigated. Thus, the melting point decreases

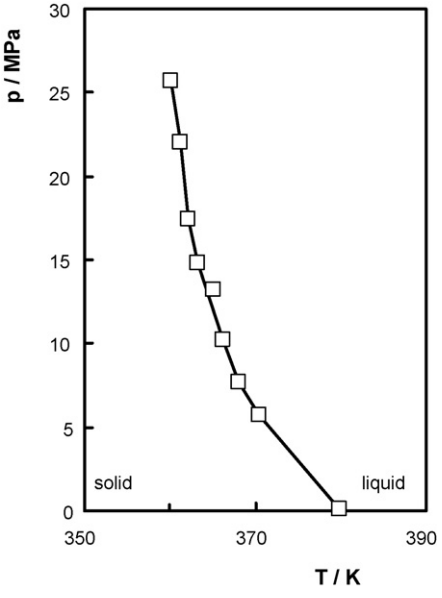

Fig. 1. Experimental SLG data for Pt(COD)Me_2/CO_2.

with increasing pressure from 378 K at 0.1 MPa to 360 K at 25.6 MPa. Therefore, an S–F two-phase equilibrium exists for temperatures from 305 K to 360 K for each pressure.

3.1.2. Solubility

The results of the solubility measurements show trends which are similar to those observed for other solids in the supercritical region. The solubility of Pt(COD)Me_2 in CO_2 increases at 313 K from 7.2×10^{-4} mol/mol at 14.3 MPa to 1.3×10^{-3} mol/mol at 29.7 MPa and from 6.6×10^{-4} mol/mol at 14.9 MPa to 3.4×10^{-3} mol/mol at 29.6 MPa and 353 K. Thus, the crossover pressure for the Pt(COD)Me_2/CO_2 system is in the range of pressures between 14 MPa and 15 MPa. Below the crossover pressure the solubility decreases with increases in temperature, and above this value the reverse is the case. The solubility is strongly influenced by the system temperature and the density of the solvent. The influences of these two variables are shown in Fig. 2 which presents the solubility of Pt(COD)Me_2 as a function of CO_2 density. The isothermal dependence of solubility on solvent density can be clearly seen. The solubility also increases with temperature at constant density primarily due to the associated increase in vapour pressure. The lines reported in the figure are the result of the empirical correlation between the logarithm of the solubility and the logarithm of the fluid density [14] following the equation:

$$\ln(y_2) = A + B \ln\left(\frac{\rho_{CO_2}}{\rho_{crit}}\right) \quad (3)$$

where y_2 is the solubility of Pt(COD)Me_2 in CO_2, A and B are constants for the system and ρ_{CO2} and ρ_{crit} are the system and critical densities of carbon dioxide, respectively. The numerical values of the constants A and B for the mixture studied together with the average absolute relative deviation (AARD) obtained are reported in Table 2. As can be seen from the AARD the data are satisfactorily correlated with this empirical relation.

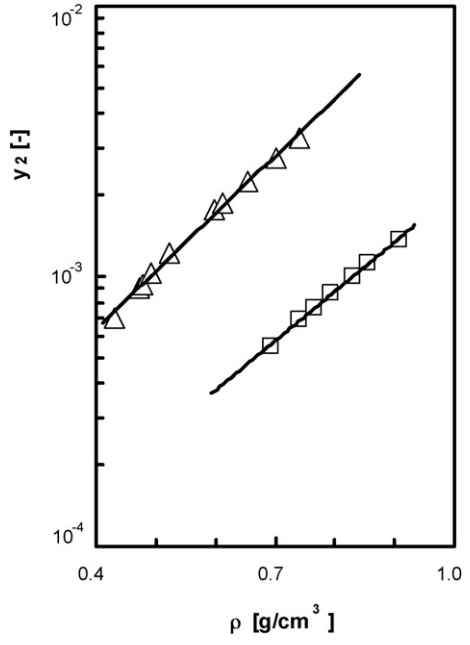

Fig. 2. Experimental solubility data for Pt(COD)Me_2 in CO_2 at 313 K (□) and 353 K (Δ). The density of CO_2 is taken from NIST Chemistry WebBook [15].

Table 2
Results of the empirical correlation of the solubility

T (K)	A	B	AARD[a] (%)
313	−8.8291	3.3604	5.81
353	−7.0353	2.8239	6.44

[a] $\mathrm{AARD}(\%) = \frac{100}{N}\sum_1^N \frac{|y_{exp} - y_{calc}|}{y_{exp}}$.

Based on experimental results reported above, the following process conditions were chosen:

(a) In order to investigate the influence of the temperature and therewith phase behaviour on the product properties, a pressure of 15.5 MPa and a temperature below (T = 353 K, SFRD 1) and above (T = 373 K, SFRD 3) the melting temperature was chosen. At such a temperature, a liquid–fluid (L–F) instead of S–F equilibrium exists and the formation of liquid droplets can already occur prior to reaction. As a consequence, large particles can be formed which are principally formed from or via the liquid phase [16].

(b) In order to investigate the influence of saturation on product properties, an additional experiment was performed at 353 K and 25 MPa (SFRD 2). From Eq. (3) it follows that increasing the pressure from 15.5 MPa to 25 MPa results in an increase in solubility from 7.85×10^{-4} mol/mol to 2.61×10^{-3} mol/mol. This leads to a lower saturation and higher dilution of the Pt(COD)Me_2/CO_2 mixture and therewith lower driving force for adsorption on the SnO_2-coated support.

3.2. Loadings of the catalysts

Table 3 summarizes the experimental pressure, temperature, and density combinations applied during supercritical deposition as well as the platinum contents of the catalysts. The Pt loading of sample SFRD 2 (0.31 wt.%) is low as compared to samples SFRD 1 (0.71 wt.%) and SFRD 3 (0.91 wt.%). As shown below, this can be explained by taking a closer look at the equilibrium solubility of Pt(COD)Me_2 in CO_2 and the saturation of the binary mixture. Thereby, the saturation is defined as the ratio of the equilibrium solubility at the

Table 3
Experimental conditions for supercritical Pt-deposition and SnO_2 and Pt content of the samples; the density data were taken from NIST data base [15]

Catalyst	p (MPa)	T (K)	ρ (g/cm^3)	SnO_2 (wt.%)	Pt[a] (wt.%)	E[b]
SFRD 1 ■	15.5	353	0.449	7.3	0.71	0.65
SFRD 2 ◆	25.0	353	0.687	6.2	0.31	0.38
SFRD 3 ▲	15.5	373	0.348	6.8	0.91	0.82
Wet dep. ●	–	–		6.3	0.43	–

[a] Platinum content determined via X-ray fluorescence.
[b] Degree of Pt deposition according to Eq. (4).

prevailing process conditions to the actual dissolved amount of $Pt(COD)Me_2$ in CO_2. The degree of Pt deposition, defined in the following equation is reduced:

$$E = \frac{m_{\mathrm{Pt,catalyst}}}{m_{\mathrm{Pt(COD)Me_2,used}}\left(\tilde{M}_{\mathrm{Pt}}/\tilde{M}_{\mathrm{Pt(COD)Me_2}}\right)} \quad (4)$$

where m_i and $\tilde{M}_i$ are the masses and molecular weights of Pt or $Pt(COD)Me_2$, respectively. The noticeable lower saturation of the supercritical mixture at higher pressure (14% instead of 64% at 15.5 MPa and 353 K) results in a decreased adsorption of the organometallic precursor due to the lower driving force at these conditions.

Although the pressure during experiments SFRD 1 and 3 was kept constant, the higher temperature during SFRD 3 results in a lower density (Table 3). This results in a decrease of the equilibrium solubility and therewith in a higher saturation of the supercritical mixture. This is most probably the reason for the higher degree of Pt deposition on catalyst SFRD 3 as compared to SFRD 1.

3.3. Surface morphology

The dip-coated layer of SnO_2 does homogeneously cover the Al_2O_3 surface of the foam. The thickness amounts to 5–10 μm along the foam struts and up to 20 μm in regions with a higher concavity. A top view on the surface (Fig. 3) of the catalyst shows more clearly the scaly structure of the SnO_2 layer. The cracks arise upon drying, when capillary forces cause a strong compression and shrinkage of the wash coat. The platinum particles were not visible on the SEM images taken from the SFRD sample (Fig. 3A), even though the presence of platinum and, of course, SnO_2 was confirmed with EDX on different analyzed spots of the wash coat, with characteristic peaks at approx. 2.1 keV and 9.4 keV. In contrast, the catalyst prepared through aqueous impregnation exhibited large Pt crystals sticking out on various locations of the SnO_2 surface, especially in the cracks of the wash coat (Fig. 3B). The EDX analysis of these crystals showed Pt peaks, only, with no SnO_2 identifiable. The analysis of the wash coat itself yields both, Pt and Sn signals.

3.4. Platinum particle size distributions

The catalyst obtained from supercritical deposition SFRD 1 and 2 shows a very narrow size distribution of platinum nanoparticles. Since no significant difference between the size distribution of the Pt particles from SFRD 1 and 2 was observed, these two catalysts were re-evaluated together giving a single platinum particle size distribution. The average diameter D of the Pt particles deposited in catalysts SFRD 1 and 2 amounts to 3.2 nm (Fig. 4).

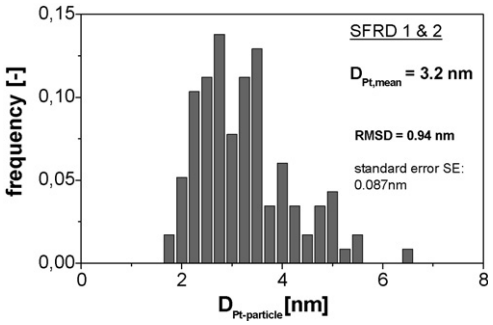

Fig. 4. Pt particle size distribution in catalysts SFRD 1 and 2 derived from 117 analyzed particles.

Neither agglomerates nor Pt crystals with diameters exceeding 7 nm were observed. Platinum could be detected in every analyzed spot of the SnO_2 layer. Fig. 5 shows a typical TEM image of catalyst SFRD 1 together with its corresponding EDX plot.

Catalyst from SFRD 3 shows a particle size distribution shifted to larger sizes than the first two, as can be seen in Fig. 6. Elongated particles were observed, reaching sizes up to 13 nm. Furthermore, some of the particles show signs of coalescence (Fig. 7), indicating the presence of a liquid phase after adsorption of the platinum complex. The high contrast of the observed Pt in this sample in comparison to the other two catalysts from supercritical deposition is a clear sign of particle growth due to coalescence. EDX-analysis of SFRD 3 shows no significant differences.

In the catalyst prepared by means of wet deposition, the Pt particles exhibit a different size and morphology. The particle size distribution is much broader. In Fig. 8, the data of Fig. 4 and the Pt-particle size distribution of the catalyst from wet deposition were merged for comparison. Although all particles with diameters >100 nm (in the catalyst made by wet deposition) were not taken into consideration, the differences between the two catalysts are quite obvious. While 7 nm is the maximum particle diameter found on sample SFRD 1 and 2,

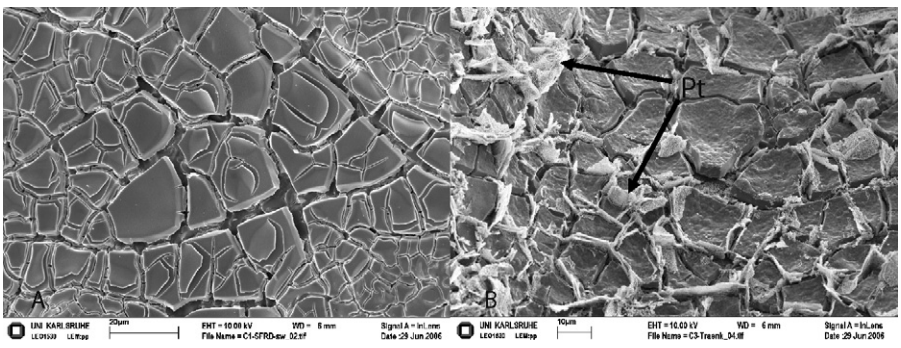

Fig. 3. SEM images of the Pt/SnO_2 surface of the catalysts: (A) sample SFRD 1 and (B) sample prepared by wet (aqueous) deposition.

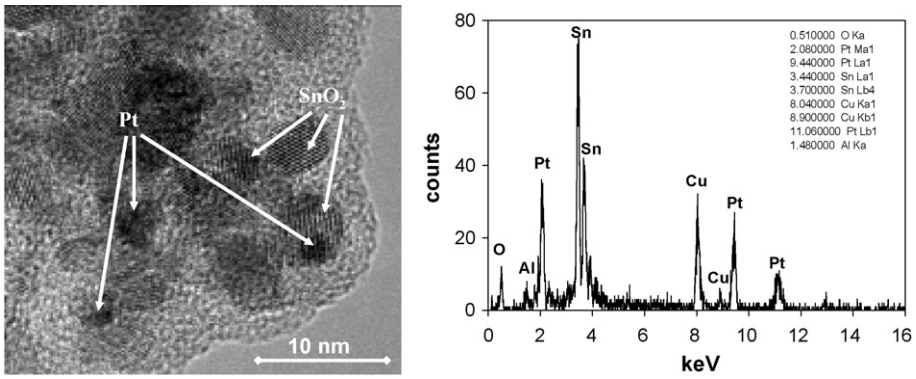

Fig. 5. TEM and EDX analysis of catalyst SFRD 1.

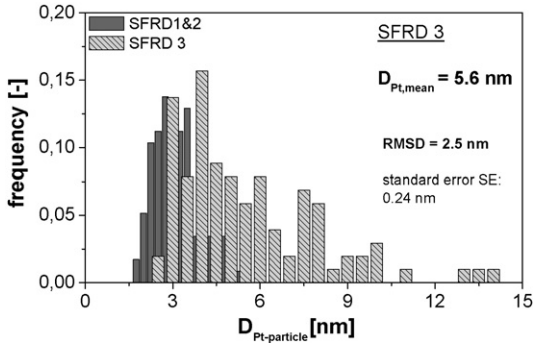

Fig. 6. Comparison of Pt size distributions between the catalyst SFRD 3 (102 analyzed particles) and the catalysts SFRD 1 and 2.

this value represents the minimum size of Pt particles on the foam loaded by wet deposition; the average diameter there amounts to 27 nm.

Within the SnO_2 phase, nanoparticles with diameters between 7 nm and 20 nm were detected (Fig. 9A). In these regions, EDX-analyses indicate slightly higher Pt peak intensities than in the case of catalyst SFRD 1. Bigger Pt crystals (Fig. 9B) and very large agglomerates with sizes up to 2 μm (Fig. 9C) were observed in areas where no tin dioxide could be found; a typical EDX-plot is depicted in Fig. 9D. These large Pt particles are probably of the same type as those visible in Fig. 3B, which are grown in the cracks and reaching out of the surface of the SnO_2 wash coat.

3.5. CO oxidation activity

Because the reaction of carbon monoxide with oxygen proceeds at the boundary between Pt and SnO_2 exposed to the gas phase, it can be anticipated that the foam loaded with Pt by means of wet impregnation shows a worse performance because it contains larger Pt particles, part of which, in addition, have no contact with SnO_2. In Fig. 10, the volumetric reaction rates of the foam catalysts (Eq. (1)) are plotted versus the gas temperature. Catalysts SFRD 1 and 2 showed high activities at moderate temperatures, reaching the region of external mass transfer limitation already at 423 K. The catalyst stemming from wet deposition exhibited a low activity below 420 K. Above 430 K, a distinct increase in reaction rate is observed until mass transfer is controlling above 473 K.

In the temperature regime, where external mass transfer is governing, it is not the intrinsic activity of the catalysts but rather their surface area, which is determining the rate. At equal bed volume and volumetric surface area, all catalysts should perform at the same rate in this transport-controlled regime. Here, all catalysts except for sample SFRD 3 approached the

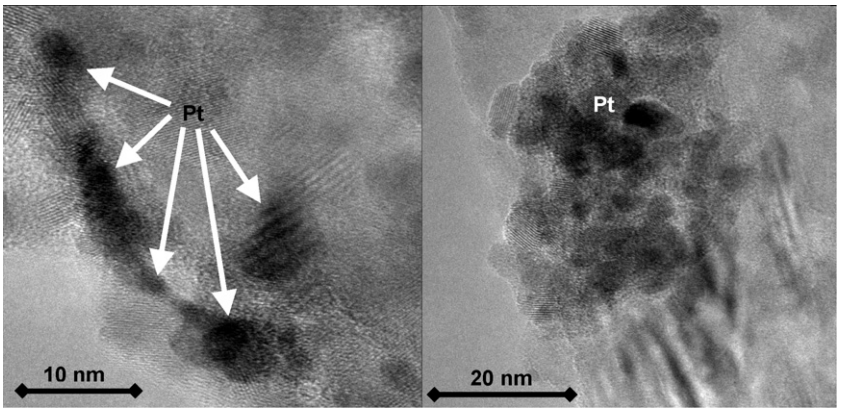

Fig. 7. TEM analysis of catalyst SFRD 3.

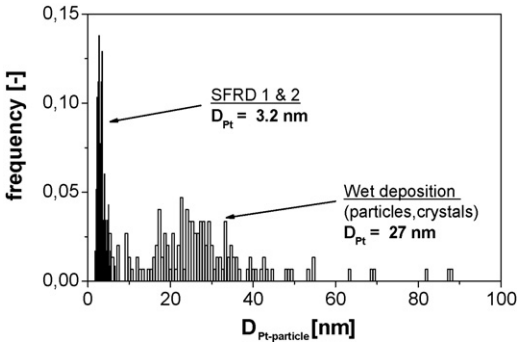

Fig. 8. Comparison of Pt size distributions between the catalyst from wet deposition (175 analyzed particles) and the catalysts SFRD 1 and 2.

same high-temperature rate. The lower rate measured over SFRD 3 is ascribed to the lower geometric surface per bed volume (S_{Geo}) of the foam piece used as carrier for this catalyst. Although all foam supports were purchased from the same manufacturer, they were not exactly uniform.

To reveal differences in the intrinsic catalytic activity of the samples, it is necessary to evaluate the data at lower temperatures when the rates are controlled by the chemical reaction rather than by the transport to the surface. Hence, only the data represented by the filled symbols in Fig. 10 were used to calculate the rate coefficients k_{Pt}. It should be noticed that these coefficients are related to the platinum content of the catalytic foams (Eq. (2)). Therefore, they reflect the intrinsic catalytic activity irrespective of the actual platinum loading.

The corresponding Arrhenius plots are depicted in Fig. 11. Obviously, the slopes of all plots, i.e. the activation energies of the catalysts, are almost the same, which could be expected in view of the similar chemical nature of the catalysts. The absolute activity levels, however, differ and follow the sequence SFRD 1 ≅ SFRD 2 > SFRD 3 > wet deposition. We ascribe these differences in activity to the diverging degrees of platinum dispersions on the catalysts as described in the previous section, which are highest in case of the samples SFRD 1 and 2, and lowest in case of the sample which was Pt-loaded by means of aqueous impregnation. In contrast to samples SFRD 1 and 2, the platinum loading of SFRD 3 was performed at conditions where the adsorbed $Pt(COD)Me_2$ could melt. A liquid phase might be formed, if the molecules of $Pt(COD)Me_2$ are dense enough to form a continuous phase on SnO_2. So if the available surface area of A_{SnO_2} (m^2) on the catalyst is smaller than the required area of the deposited molecules of the organometallic, a liquid phase would form on the SnO_2-layer. The available area for adsorption can be calculated as follows:

$$A_{SnO_2} = m_{cat} w_{SnO_2} S_{BET,SnO_2} = 6.44\,m^2 \quad (5)$$

with w_{SnO_2} (wt.% of SnO_2) = 6.5% and S_{BET,SnO_2} (BET surface area) = 118 m^2/g (S_{BET,Al_2O_3} = 0.18 m^2/g, negligible).

With the modeling software Cerius^2 (Accelrys), the molecular structure of $Pt(COD)Me_2$ could be reconstructed. The energetic most favorable atomic arrangement of the

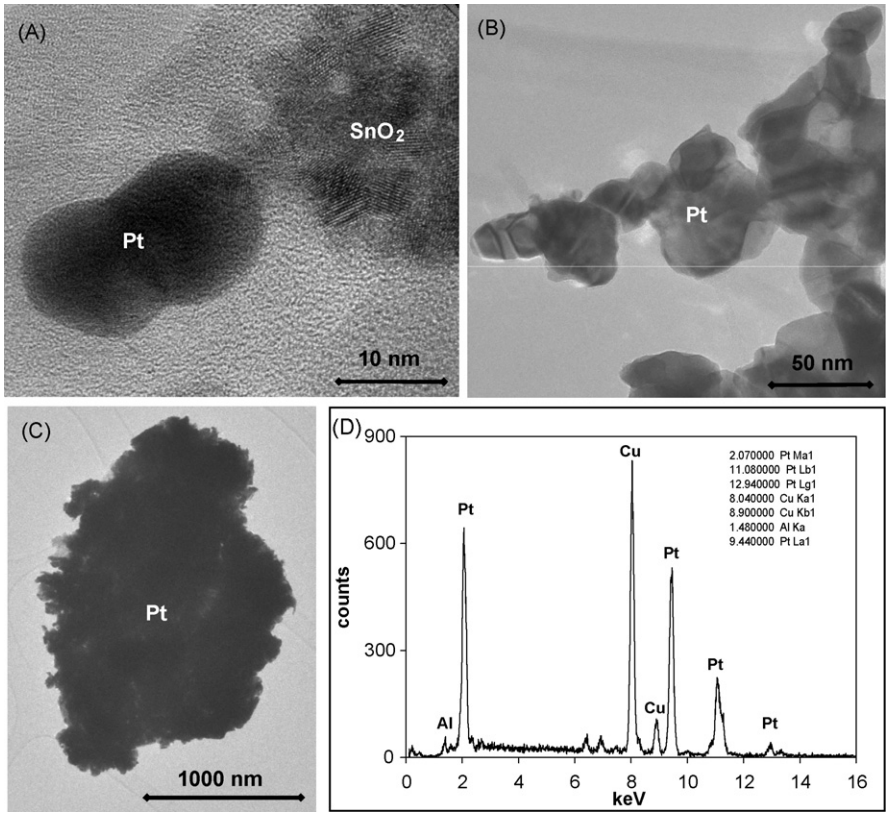

Fig. 9. TEM and EDX analysis of wet deposition catalyst: nanoparticle (A), crystals (B) and agglomerate (C); EDX-spectra of the region with agglomerated crystals (D).

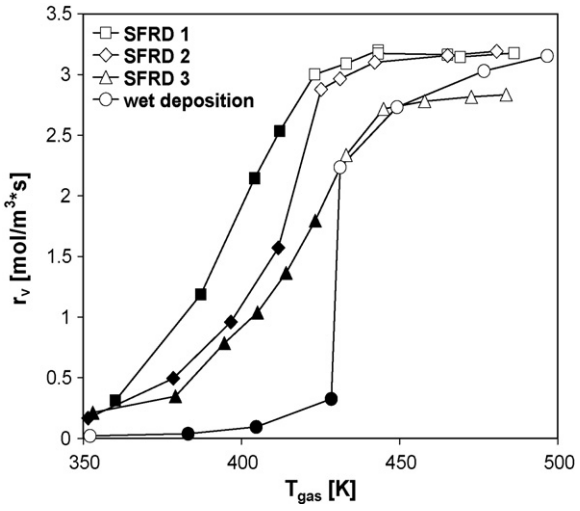

Fig. 10. Volumetric reaction rate of foam catalysts as a function of the gas temperature; filled symbols: chemical rate-controlled kinetic regime (data taken for plotting rate coefficients in Fig. 11); open symbols: mass transfer-controlled regime.

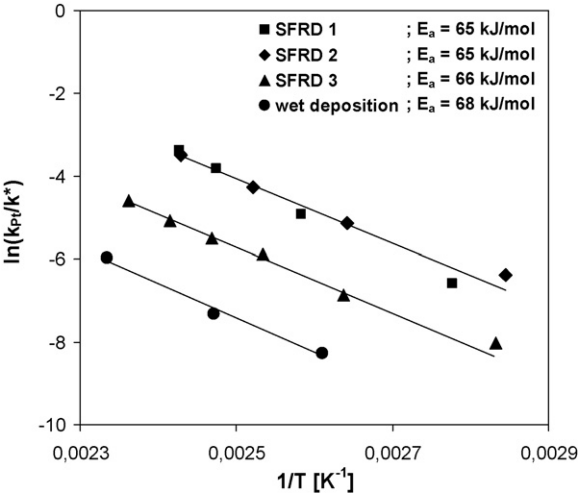

Fig. 11. Arrhenius plots of the CO oxidation in the regime of chemical rate control; E_a is the activation energy.

organometallic was calculated giving the surface and volume of the molecule and its diameter: 0.8 nm. The required area for an adsorbed complex molecule can be then calculated to:

$$A^{\text{molecular}}_{\text{Pt(COD)Me}_2} = \frac{\pi}{4} D^2_{\text{molecule}} = 0.503\,\text{nm}^2 \quad (6)$$

With the molecular weight of the organometallic (333.34 g/mol), the required area per gram can be calculated to

$$S^{\text{mass}}_{\text{Pt(COD)Me}_2} = \frac{A^{\text{molecular}}_{\text{Pt(COD)Me}_2} N_A}{\tilde{M}_{\text{Pt(COD)Me}_2}} = 908.72\,\text{m}^2/\text{g} \quad (7)$$

giving the total required area:

$$A_{\text{Pt(COD)Me}_2} = S^{\text{mass}}_{\text{Pt(COD)Me}_2} m_{\text{cat}} w_{\text{Pt}} \frac{\tilde{M}_{\text{Pt(COD)Me}_2}}{\tilde{M}_{\text{Pt}}} = 11.87\,\text{m}^2 \quad (8)$$

Since $A_{\text{Pt(COD)Me}_2}$ is higher than A_{SnO_2}, a continuous (bulk) phase of Pt(COD)Me_2 is formed after adsorption, which most probably melts at experimental conditions. The formation of the liquid phase causes coalescence of Pt-complex molecules on the SnO_2-layer, leading to larger Pt particles after reduction (confirmed with TEM) and thus affecting the dispersion of the noble metal on SnO_2 and with it the activity of the catalyst.

4. Conclusions

Supercritical fluid reactive deposition is an appropriate and convenient method to deposit metallic nanoparticles on catalyst supports. The main advantages are its flexibility regarding the carrier and the washcoat, low processing temperatures and the absence of any contaminants like chlorine in the ready-to-use catalyst. A prerequisite is the knowledge of the thermodynamic behaviour of the supercritical solution containing the metallorganic complex. For Pt(COD)Me_2 in carbon dioxide, we investigated the phase behaviour and the solubility to determine the optimum temperature and pressure range for SFRD of platinum. Ceramic foams coated with a layer of tin dioxide were used as supports. As compared to the conventional deposition of Pt by means of aqueous impregnation, SFRD yielded considerably smaller Pt particles in a much narrower size distribution. In the oxidation of carbon monoxide, the SFRD catalysts with the high Pt dispersion exhibited superior activity as compared to the sample with impregnated Pt.

Acknowledgements

This project was financed by the German Research Foundation (DFG). One of the authors (S.Y.) thanks the state Baden-Wuerttemberg for the financial support in form of a fellowship.

References

[1] R.J. Farrauto, Y. Liu, W. Ruettinger, O. Ilinich, L. Shore, T. Giroux, Catal. Rev. 49 (2007) 141–196.
[2] K. Grass, H.-G. Lintz, J. Catal. 172 (1997) 446–452.
[3] D.R. Schryer, B.T. Upchurch, B.D. Sidney, K.G. Brown, G.B. Hoflund, R.K. Herz, J. Catal. 130 (1991) 314–317.
[4] C.J. Wright, C.F. Sampson, UK Patent GB 2134004 B (1986).
[5] Y. Zhang, C. Erkey, J. Supercrit. Fluids 38 (2006) 252–267.
[6] G.M. Schneider, Fluid Phase Equilibr. 10 (1983) 141–157.
[7] K.S. Morley, P.C. Marr, P.B. Webb, A.R. Berry, F.J. Allison, G. Moldovan, P.D. Brown, S.M. Howdle, J. Mater. Chem. 12 (2002) 1898–1905.
[8] J.J. Watkins, J.M. Blackburn, T.J. McCarthy, Chem. Mater. 11 (1999) 213–215.
[9] Y. Zhang, D. Kang, C. Saquing, M. Aindow, C. Erkey, Indian Eng. Chem. Res. 44 (2005) 4161–4164.
[10] M. Türk, G. Upper, P. Hils, J. Supercrit. Fluids 39 (2006) 253–263.
[11] M. Türk, G. Upper, M. Steurenthaler, K. Hussein, M.A. Wahl, J. Supercrit. Fluids 39 (2007) 435–443.
[12] K. Grass, H.-G. Lintz, G. Poncelet, J. Martens, B. Delmon, P.A. Jacobs, in: P Grange (Ed.), Studies in Surface Science and Catalysis-91: Preparation of Catalysts VI, Elsevier, Amsterdam, 1995, pp. 1111–1119.
[13] R.M. Lemert, K.P. Johnston, Fluid Phase Equilibr. 45 (1989) 265–286.
[14] S.K. Kumar, K.P. Johnston, J. Supercrit. Fluids 1 (1988) 15.
[15] http://webbook.nist.gov/chemistry/fluid/.
[16] A. Diefenbacher, M. Türk, J. Supercrit. Fluids 22 (2002) 175–184.